

Synthetic Turbulence Generators for RANS-LES Interfaces in Zonal Simulations of Aerodynamic and Aeroacoustic Problems

Michael L. Shur · Philippe R. Spalart ·
Michael K. Strelets · Andrey K. Travin

Received: 16 August 2013 / Accepted: 25 February 2014
© Springer Science+Business Media Dordrecht 2014

Abstract The paper presents the detailed formulation and validation results of simple and robust procedures for the generation of synthetic turbulence aimed at providing artificial turbulent content at the RANS-to-LES interface within a zonal Wall Modelled LES of attached and mildly separated wall-bounded flows. There are two versions of the procedure. The aerodynamic version amounts to a minor modification of a synthetic turbulence generator developed by the authors previously, but the acoustically adapted version is new and includes an internal damping layer, where the pressure field is computed by “weighting” of the instantaneous pressure fields from LES and RANS. This is motivated by the need to avoid creating spurious noise as part of the turbulence generation. In terms of pure aerodynamics, the validation includes canonical shear flows (developed channel flow, zero pressure gradient boundary layer, and plane mixing layer), as well as a more complex flow over the wall-mounted hump with non-fixed separation and reattachment, with emphasis on a rapid conversion from modeled to resolved Reynolds stresses. The aeroacoustic applications include the flow past a trailing edge and over a two-element airfoil configuration. In all cases the methodology ensures a very acceptable accuracy for the mean flow, turbulent statistics and, also, the near- and far-field noise.

Keywords Zonal RANS-LES · Turbulent content at RANS-LES interface · Attached and mildly separated flows · Aeroacoustics

M. L. Shur · M. K. Strelets (✉) · A. K. Travin
Saint-Petersburg State Polytechnic University, Saint-Petersburg, Russia
e-mail: strelets@mail.rcom.ru

M. L. Shur · M. K. Strelets · A. K. Travin
New Technologies and Services, LLC, Saint-Petersburg, Russia

P. R. Spalart
Boeing Commercial Airplanes, Seattle, USA

1 Introduction

A certain trend in Computational Fluid Dynamics and Aeroacoustics (CFD and CAA) is away from empirical and semi-empirical methods, towards methods based on first principles. As far as aerodynamics is concerned, this implies turbulence-resolving approaches (TRA) ranging from Direct Numerical Simulation (DNS) and Large-Eddy Simulation (LES) to different hybrid RANS-LES approaches. A fundamental advantage of such approaches over, e.g., the RANS-based semi-empirical methods which remain workhorses in both areas, is that they are much less dependent on empirical information, thus giving hope of a reliable prediction of flow and noise characteristics away from calibration conditions. Other than that, they allow a deeper understanding of basic flow physics and noise generation mechanisms. This has motivated a wave of new studies employing TRA for a wide range of aerodynamic and aeroacoustic problems. For flows at realistic (high) Reynolds numbers, the most widely used TRA are hybrid RANS-LES approaches, which is explained by their relatively low computational cost (compared to a full LES), on one hand, and acceptable accuracy for a wide range of applications, on the other hand. However, the true capabilities of hybrid methods depend on both the type of flow in question, and the peculiarities of the specific method used.

In massively separated flows (e.g., flows past landing gear, cavities or airfoils, beyond stall, at high angles of attack), independently of the state of the attached turbulent boundary layer, a rapid spontaneous transition to turbulence (sometimes called “secondary transition”) occurs in the separated shear layer(s) caused by a strong “new” instability, and it is precisely the turbulent structures formed in these shear layers and in recirculation zones which are responsible for the major aerodynamic characteristics and, especially, for the noise produced by the flow. This makes it unnecessary to resolve turbulence in the attached boundary layer, thus significantly facilitating the simulation of such flows and, in particular, justifying the use of the original Detached Eddy Simulation (DES) approach [1] and its more recent modifications (“DES-like” approaches), e.g., DDES [2] and IDDES [3]. A positive feature of these approaches is that they are non-zonal or “global”, i.e., they are applied to the whole flow-field without a priori specification of the RANS and LES regions, or imposing any artificial turbulent fluctuations at the RANS-LES interface.

In attached and mildly separated flows (e.g., flows over trailing edges and flaps) the situation is quite different. In this case the overall aerodynamics and noise produced by the flow are crucially dependent on the turbulent vortical structures which populate the attached boundary layers or shallow separation zones, where the non-zonal DES-like hybrid methods are known to be less accurate. So, strictly speaking, the only TRA capable of a truly accurate representation of turbulence in such flows is the full “well-resolved” LES (ensuring resolution of turbulent structures down to the wall), possibly even including prediction of laminar-turbulent transition. However at realistic Reynolds numbers, this approach is not affordable today and will not become affordable in the foreseeable future [1]. As a result, zonal/embedded LES (actually, zonal Wall Modeled LES - WMLES) with a priori specification of RANS and LES sub-domains and the imposition of artificially created turbulence at their interface (LES inflow) appears to be the only practical tool capable of ensuring a reliable prediction of aerodynamic and acoustic characteristics of such flows.¹

¹Note that application of embedded LES may be helpful also for massively separated flows, where it can considerably reduce the so called “grey area” causing a delay of transition to turbulence in the separated shear layers the global methods are known to suffer from [5].

The necessity of injecting turbulence at the RANS-LES interface is caused by the inevitable existence of an “adaptation region” required to establish “mature” turbulence in the LES downstream of the interface. Without resolved turbulence at the LES inflow, this region turns out to be too long and damages the whole solution. Therefore, devising a physically realistic and computationally efficient way of creating turbulent content at the RANS-LES interface in zonal LES is of crucial importance for the overall success of this approach.

As of today, even for purely aerodynamic applications this problem is far from solved, and is an area of intensive research. Note that the artificial nature of the “turbulence” created at the interface makes a complete elimination of the adaptation region hardly possible. The problem of suppression of spurious noise sources at the RANS-LES interface caused by an abrupt appearance of unsteady vortical structures is even more challenging. So, the objective of the research is to find ways to minimize these negative effects.

In this paper we outline a simple and rather efficient method for the generation of turbulent content within zonal LES, which presents an improved version of the purely aerodynamic Synthetic Turbulence Generator (STG) proposed by Adamian et al. [4], adapted to aeroacoustic applications. The paper is organized as follows.

We start with a brief overview of existing methods for creating turbulent content at the LES inflow in zonal RANS-LES (Section 2). Then in Section 3 a detailed formulation of the proposed method is given, and results of the solution of a set of aerodynamic and aeroacoustic problems obtained with the use of the zonal IDDES approach coupled with this method are presented and discussed in some detail. Finally in Section 4 some concluding remarks are presented.

2 Overview of Existing Approaches

This is a very active research area. The wide range of techniques for creating turbulent content at the LES inflow within the zonal approaches available in the literature can be roughly divided into five classes: 1) precursor DNS or LES; 2) turbulence recycling; 3) “synthetic” turbulence; 4) artificial forcing or volume source terms; 5) vortex generating devices. Some of these classes (particularly the synthetic turbulence approach) include a large number of techniques, and can be divided into several subclasses with rather different properties. Below we briefly consider all five classes and their pros and cons. However before doing this, it is necessary to dwell upon different procedures for coupling RANS and LES applied in the framework of zonal LES. These can be divided into two large groups: two-stage (semi-coupled) and one-stage (fully coupled) procedures.

Within the semi-coupled approaches, illustrated by left frame in Fig. 1, simulations are carried out in two stages. In the first stage, a RANS solution of the flow in question is performed in the whole computational domain, and in the second stage, LES is conducted only in an LES sub-domain. In this case the boundary conditions for the velocity at the RANS-LES interface are usually specified by imposing velocity values equal to those from RANS, often with added artificial (“turbulent”) fluctuations. In compressible simulations, the temperature at the interface is typically set equal to that from the RANS solution, but sometimes temperature fluctuations are also imposed (see Garnier et al. [6] for more details). Finally, boundary conditions for pressure depend on the Mach number at the interface. For a supersonic flow, the pressure set equal to that in the RANS solution and for subsonic or incompressible flow it is extrapolated from the interior of the LES sub-domain. The approach can be called “semi-coupled” because this procedure involves only “one-way”

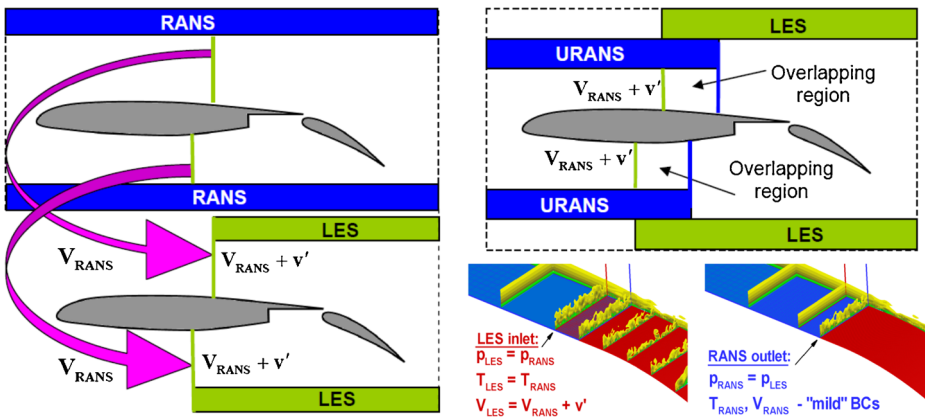


Fig. 1 Schematics of two-stage semi-coupled (*left*) and one-stage fully coupled (*right*) zonal RANS-LES strategies

coupling of the solutions in the RANS and LES regions (in the direction from RANS to LES, but not vice versa).

In the framework of the fully coupled approaches, schematically shown in the right frame of Fig. 1, Unsteady RANS (URANS) and LES are simultaneously performed in the RANS and LES sub-domains respectively (this implies that the two sub-domains overlap). Other than that, in this case, along with the boundary conditions at the LES inlet, some conditions should be also imposed to the URANS at its outlet boundary.

Typically, the unsteady boundary conditions at the LES inlet are similar to those described above for the semi-coupled approach. The difference is that in this case the required flow quantities at the interface are “borrowed” from the current URANS solution (either the instantaneous solution at the previous time step, or its running time-average). Other than that, considering that the LES inlet is, in fact, an inter-block boundary of a multi-block grid, one can set pressure equal to that in RANS solution even in a subsonic/incompressible flow.

At the RANS outlet, the pressure is set equal to that from the available LES solution or its running average for subsonic/incompressible flow. All the other flow variables are extrapolated from the interior of the RANS sub-domain. In a supersonic flow extrapolation is applied to all the variables including pressure. This implies that not only the RANS-LES interface but also the RANS outlet should be placed in the attached flow region, which is non-trivial in simulations of complex 3D flows.

The two procedures outlined above are rather different and have their own pros and cons. Two important advantages of the fully coupled approach are the feedback between the LES and URANS domains which makes it more tolerant to the interface location (allowing its placement in the relatively close vicinity of “sensitive” areas which require the use of TRA) and having no need for a precursor RANS solution in the whole domain, except maybe for initialization purpose. Also, LES is more accurate than RANS in massively-separated regions, so that the joint solution is normally more accurate than the pure RANS solution could be. On the other hand, the two-stage approach is more tolerant to grid topology and does not require an overlapping grid capability in the code. This method is more adequate when the LES is conducted even though the RANS is accurate, but to generate unsteady data in a sub-region, typically to predict vibrations and noise.

In any case a key common element of both approaches is a procedure to create turbulent velocity fluctuations \mathbf{v}' at the RANS-LES interface, and the performance of this procedure strongly influences the success of the method as a whole. The reason is that no artificial turbulence fluctuations can reproduce *all* the characteristics of the real turbulence and, therefore, any algorithm for their generation is inevitably imperfect and presents a compromise between accuracy, robustness, complexity of implementation, and computational cost.

In terms of accuracy and functionality, the algorithm should shorten as much as possible the “adaptation region” needed to establish “mature” boundary-layer turbulence in the LES downstream of the interface. It is also very desirable for this property (a short adaptation region) not to be limited to the simplest flows, e.g., zero pressure gradient boundary layers (ZPG BL), since this would be very restrictive in terms of location of the RANS-LES interface in complex flows. Other than that, the algorithm is likely to perform equally well in DNS, well-resolved LES, and WMLES. Finally, for aeroacoustic problems, it is of primary importance to avoid introducing intense spurious noise sources, which would corrupt the genuine acoustic field generated by the flow. However, an inherent feature of virtually all of the existing approaches is the sudden formation of energetic vortical structures at the RANS-LES interface, which inevitably generates strong spurious noise. Most methods in fact violate the instantaneous continuity equation, if the RANS and LES fields are taken as one, due to the discontinuity of velocity. Therefore, if it is applied to aeroacoustics, any basic “aerodynamic” algorithm for imposing unsteady turbulent content at the LES inflow should be supplemented by some means of suppressing this spurious noise.

In terms of “design”, the algorithms for generation of fluctuations should be coding-friendly and computationally inexpensive, should use only those turbulence characteristics that are available from the conventional RANS models (k, ε, ω , Reynolds stresses), and should not be limited to any specific grid type (structured/unstructured) or topology.

Considering that no known method of creating artificial turbulence can satisfy *all* the demands formulated above (even if the specific “aeroacoustic” demands are disregarded), the available methods should be assessed by their overall closeness to such an “ideal” method. For the sake of definiteness, our assessment below is conducted in the framework of the single-stage fully coupled methodology.

2.1 Precursor DNS or LES

In this method (see schematic in Fig. 2a) the velocity fluctuations \mathbf{v}' at the RANS-LES interface are set equal to normalized/rescaled fluctuations from a precursor/auxiliary DNS or well-resolved LES of some “canonic” flow (e.g., developed channel flow or flat plate boundary layer) or from corresponding databases. Provided that rescaling laws are correct, it creates realistic turbulence at the RANS-LES interface and, therefore, ensures a high accuracy of the simulation. However, the method is not self-sufficient (since it relies upon external databases) and has been rather restricted in terms of the Reynolds number, which makes its applicability to complex (far from the canonical) high Reynolds number flows questionable (the authors are aware of only one application of a precursor LES to simulation of a complex flow within zonal LES [7]). Other than that, the method is rather computationally expensive in terms of both CPU and memory load. Finally, most precursor simulations have rather narrow domains with periodic conditions, whereas many flows in valuable geometries will have a wide domain, compared with the boundary-layer thickness. Thus, the precursor data would have to be artificially repeated, and unless the flow

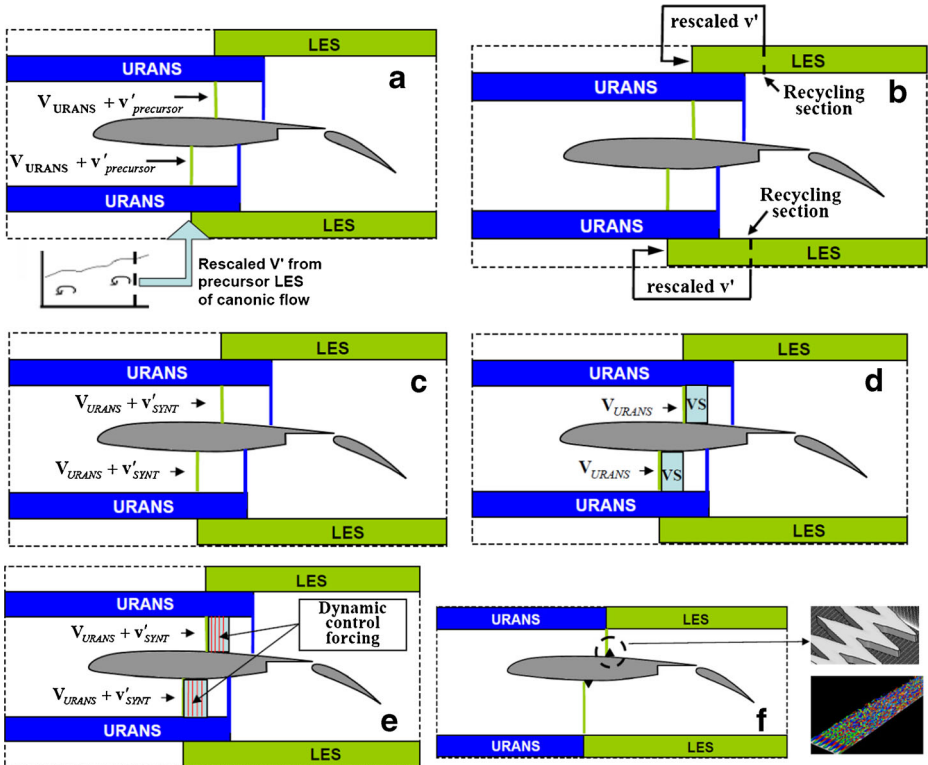


Fig. 2 Different approaches to specifying velocity fluctuations at LES inflow

is perfectly uniform in the lateral direction with a 2D geometry, repeated with unnatural discontinuities.

2.2 “Recycling” of turbulence

The idea of this method belongs to Lund et al. [8] who proposed a formulation of the inlet conditions in pure LES and DNS based on transferring to the LES inlet the unsteady content available in the same simulation at some downstream (“recycling”) section of the flow (see Fig. 2b).

For flows evolving in the streamwise direction this implies an appropriate rescaling of the transferred turbulence, which can be far from trivial. A key distinction is whether this evolution only concerns a slow growth of the boundary-layer thickness, or also a gradient in the edge velocity and pressure. However, when a reliable rescaling is possible, this technology “creates” turbulence of high quality resulting in a rather short adaptation distance (a few times the boundary layer thickness, δ_{BL}). Moreover, more robust/general versions, e.g. those proposed by Spalart et al. [9], Shur et al. [10], and Araya et al. [11] allow a tangible widening of the domain of applicability of the original formulation [8] thanks to more general rescaling procedures and an adaptation to the fully coupled RANS-LES methods. As a

result, when applicable, recycling of turbulence is a rather efficient tool for creating turbulent content at the RANS-LES interface, and its “rating” in terms of matching the general demands to such procedures is considerably higher than that of the precursor DNS/LES.

However, the approach still has rather severe constraints in terms of flow complexity because of the difficulty of adequate rescaling in the presence of strong pressure gradients. Other than that, it also requires some special initialization to ensure the rapid establishment of mature turbulence within the recycling region after starting the simulation, i.e., it is not quite self-sufficient. For aeroacoustic applications, a more important fact is that the method has the undesirable secondary effect of introducing nonphysical peaks into the spectrum of generated turbulence at the recycling frequency $f_{recycl} \approx U_{conv}/L_{recycl}$ (U_{conv} being the characteristic convection velocity) - see Section 3.1.2 below.² This issue of periodic cycles in the solution is well-known.

2.3 “Synthetic” turbulence generation

This approach, which implies superimposing some externally-generated artificial (“synthetic”) turbulent velocity fluctuations onto the (U)RANS velocity field at the RANS-LES interface (Fig. 2c), is currently considered as more suitable for the simulation of complex industrial flows than using precursor simulations or recycling of turbulence. As already mentioned, the number of available methods of this type is rather large, ranging from the simplest generators based on white random noise to rather complicated ones employing information not only on the time averaged characteristics and turbulence statistics available from RANS, but also on time- and space-correlations. Their attractive features include self-sufficiency, relative ease of implementation, computational efficiency, and, last but not least, tolerance to grid type and topology. However, the artificial nature of the created turbulence often results in a rather long adaptation region. In other words, the accuracy of STG’s crucially depends on the “quality” of the turbulence (its closeness to real turbulence), which in turn, depends upon the specific properties of the STG used (detailed reviews of currently existing STG’s are available, e.g., in Sagaut et al. [13], Keating et al. [14], Keating et al. [15], Tabor and Baba-Ahmadi [16], and Xie and Castro [17]). For instance, the simplest and most easily implemented random (white noise) STG’s, even when they match prescribed Reynolds stresses, result in an adaptation length assessed by the evolution of the skin-friction coefficient of about 50 boundary layer thicknesses [8] and therefore are almost completely useless as inlet conditions. The reason is that the turbulence lacks correlation in all directions, and much of the small-scale content rapidly dies out. As an improvement, a wide class of STG’s has been developed based on digital filtering or creating coherent turbulent structures with specified sizes and shapes (Klein et al. [18], Di Mare et al. [19], Kornev and Hassel [20], Veloudis et al. [21], Xie and Castro [17], Jarrin et al. [22], Jarrin et al. [23], Mathey et al. [24], Pamies et al. [25]). Although they are more difficult to implement, these methods are much more accurate and achieve adaptation lengths ranging from about 20 down to 5–6 [25] boundary-layer thicknesses. Finally, another wide group of STG’s is based on an idea due to Kraichnan [26] of a superimposition of spatiotemporal Fourier modes with random amplitudes and phases (Smirnov et al. [27], Batten et al. [28],

²A way of reducing this effect as applied to LES of supersonic flat plate boundary layer has been proposed by Morgan et al. [12] but it is rather complicated, since it involves several ad hoc controlling parameters, and heavily relies on using structured grids.

Huang et al. [29], Adamian et al. [4]). It brings the adaptation of the skin-friction down to 2–4 [4] boundary layer thicknesses.

2.4 Artificial forcing

Two different approaches of this type have been proposed, both closely related to STG methods.

The first approach employed by Gritskevich and Garbaruk [30] is based on introducing in the governing equations specially designed Volume Source (VS) terms which are activated in some volume within the RANS-LES overlapping region (see Fig. 2d) and are aimed at creating at the downstream end of this area the same artificial turbulence as that created by an STG [4] applied at the RANS-LES interface. Thus, there is now a continuous velocity field, but with a momentum source. A major “technological” advantage of this approach compared to the STG methods is its compatibility with any types of grids (VS may be activated in an arbitrary set of grid cells so that the RANS-LES interface does not even need to form a grid surface). Other than that, the approach has a high potential in terms of adaptation to aeroacoustic problems thanks to the possibility of a gradual increase of the strength of the VS in the downstream direction, allowing a reduction of the spurious noise caused by the abrupt emergence of turbulence typical of the other methods. Yet, as of today, the method has been tested only for the special case of the source with a thickness in the streamwise direction equal to one computational cell, i.e., when it is nearly equivalent to an STG [4]. With a finite thickness, the VS will need to properly propagate if it is to smoothly create the LES content.

Approaches of the second of the two abovementioned types (see Fig. 2e) present a combination of STG at the RANS-LES interface, and Dynamic Control Forcing techniques (STG-DCF). These introduce closed-loop control. The idea is to introduce volume sources in a set of “control planes” downstream of the interface with a strength proportional to the difference between the running time-average and some desirable (“target”) values of some quantity known from RANS (typically, the shear or wall normal stress), thus ensuring a rapid adjustment of the synthetic turbulence generated by the STG to the real one, independently of the specific STG being used. Note, however, that a significant decrease of the adaptation length produced by STG-DCF methods compared to the pure STG ones is reached, but at the cost of a considerable increase of implementation complexity and CPU cost.

A first STG-DCF method was proposed by Spille-Kohoff and Kaltenbach [31] and tested on zonal RANS-LES of the flat plate boundary layer. The method combined DCF with a random STG and was able to reduce the adaptation length down to about $6\delta_{BL}$. De Prisco et al. [32] developed an improved DCF procedure coupled with an STG [18], which significantly enhanced computational robustness of the technique and extended it to flows with strong pressure gradient. Laraufie et al. [33] combined DCF with a modified Synthetic Eddy Method (SEM) [25] and adapted the procedure to approaches relying upon WMLES rather than well-resolved LES in the LES sub-domain of zonal LES. In both studies an almost immediate establishment of mature turbulence downstream of the DCF region was observed. However, this region itself was rather long ($\approx 20\delta_{BL}$ in [32] and $8.5\delta_{BL}$ in [33]), so that in a significant pressure gradient, the target values will become much more difficult to calculate. Finally, Roidl et al. [34, 35] used DCF techniques in combination with the original SEM [22, 23] and demonstrated good performance for transonic airfoil and supersonic boundary layer (the adaptation length in both cases was about $(2-3)\delta_{BL}$).

2.5 Vortex generating devices

The idea of this method (see Fig. 2f) proposed recently by M. Terracol (personal communication, October 2012) is to trigger the development of turbulent content at the RANS-LES interface by placing there a Vortex-Generating Device (VGD) loosely similar to those used for tripping boundary layers in experiments (to avoid a global alteration of the flow, the thickness of the VGD should be significantly less than that of the boundary layer). Advantages of a VGD over other methods include the absence of constraints in terms of flow complexity, low computational cost, and simplicity of implementation (at least if combined with the immersed boundary method, which is defendable since the exact shape of the VGD is not crucial). Other than that, the approach is much “quieter” than all the methods of creating turbulent content at RANS-LES interface considered above and, therefore, has a high potential for aeroacoustic problems. On the other hand, as of today, the method results in relatively long adaptation region (more than $10\delta_{BL}$), which makes it non-competitive with the best methods for purely aerodynamic problems. Note that this adaptation length is similar to the length for real, physical trip devices. Also, choosing an optimal VGD shape and size may not be easy.

Based on the brief overview of existing methods for creating turbulent content at the RANS-LES interface presented above, the following major conclusions can be drawn.

The area is rapidly evolving due to its high practical importance for many research and industrial applications. In terms of aerodynamics, at least for relatively simple flows, existing methods are, in principle, capable of creating realistic turbulent content at the RANS-LES interface, with an adaptation length of only $(2 - 4)\delta_{BL}$ for the best methods. However the methods differ significantly from each other in terms of complexity, accuracy, and generality. So, in this stage, it is impossible to give a definite preference to one of them. Unfortunately, none of existing aerodynamic methods “as is” (except maybe for the VGD method, which has other disadvantages) is capable of providing acceptable accuracy for aeroacoustic problems. As discussed, their common feature is a “sudden” formation of strong vortical structures accompanied with an unsteady mass source at the RANS-LES interface, which generate spurious noise, and the risk of drastically corrupting the genuine aerodynamic noise of the flow. So some special acoustically-oriented modifications of the existing methods are needed. An example of such a modification is the acoustic version of the STG method [4] presented in Section 3.2 below.

3 STG Formulation and Validation

3.1 Aerodynamic version of the method

The method, of which the original version is presented in [4], employs ideas of Kraichnan [26] and has many common features with the STG’s of Bechara et al. [36], Smirnov et al. [27], Batten et al. [28], and Billson et al. [37]. However, unlike these methods, it is capable of a plausible representation of the anisotropy of the vortical structures, which is an essential feature of near-wall turbulence.³ Other than that, it is free of the de-correlation issue inherent to the STG’s which rely on the local definition

³Method [28] is also capable of reproducing anisotropy in length scales, but only with RANS models capable of providing realistic second moments.

of turbulence length- and time-scales involved in the wavelength scaling. In this section, for the sake of completeness, we present a detailed formulation of a slightly modified method relative to [4] and then (section 3.2) outline its acoustically adapted version.

3.1.1 Formulation

Similarly to other STG methods, the velocity vector at a point $\mathbf{r} = \{x, y, z\}$ of the RANS-LES interface is specified as:

$$\mathbf{U}(\mathbf{r}, t) = \mathbf{U}_{RANS}(\mathbf{r}) + \mathbf{u}'(\mathbf{r}, t), \quad (1)$$

where $\mathbf{U}_{RANS}(\mathbf{r})$ is the mean velocity vector available from the RANS solution, and $\mathbf{u}'(\mathbf{r}, t)$ is the vector of velocity fluctuations.

Again similarly to many other methods, $\mathbf{u}'(\mathbf{r}, t)$ is defined so that the corresponding second moment tensor $\langle u'_i u'_j \rangle$ at the LES inflow is equal to the Reynolds stress tensor, $\widehat{\mathbf{R}}$, which is also assumed to be known from RANS.⁴ This is achieved by using a Cholesky decomposition of the Reynolds stress tensor, $\widehat{\mathbf{R}} = \widehat{\mathbf{A}}^T \widehat{\mathbf{A}}$, where

$$\widehat{\mathbf{A}} = \{a_{ij}\} = \begin{pmatrix} \sqrt{R_{11}} & 0 & 0 \\ R_{21}/a_{11} & \sqrt{R_{22} - a_{21}^2} & 0 \\ R_{31}/a_{11} & (R_{32} - a_{21}a_{31})/a_{22} & \sqrt{R_{33} - a_{31}^2 - a_{32}^2} \end{pmatrix}, \quad (2)$$

And the $R_{ij} = \langle u'_i u'_j \rangle$ are the components of the Reynolds stress tensor. This matrix is filled sequentially, starting from the upper left corner.

Then, the velocity fluctuations $\mathbf{u}'(\mathbf{r}, t)$ in Eq. 1 can be expressed via the components of the tensor $\widehat{\mathbf{A}}$ in the form

$$u'_i(\mathbf{r}, t) = a_{ij} v'_j(\mathbf{r}, t), \quad (3)$$

where $v'_j(\mathbf{r}, t)$ are the components of the auxiliary vector of fluctuations, which satisfies the restrictions $\langle v'_i \rangle = 0$ and $\langle v'_i v'_j \rangle = \delta_{ij}$, so that the Reynolds stresses are correct thanks to the definition of $\widehat{\mathbf{A}}$. Thus the problem of the definition of $\mathbf{u}'(\mathbf{r}, t)$ in Eq. 1 reduces to the definition of the auxiliary vector $\mathbf{v}'(\mathbf{r}, t)$. This is done by a superposition of weighted spatiotemporal Fourier modes:

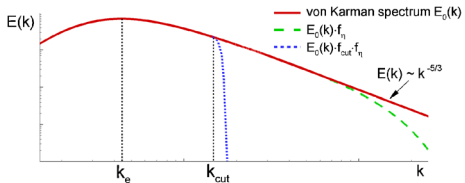
$$\mathbf{v}'(\mathbf{r}, t) = 2\sqrt{3/2} \sum_{n=1}^N \sqrt{q^n} [\sigma^n \cos(k^n \mathbf{d}^n \cdot \mathbf{r}' + \varphi^n)]. \quad (4)$$

Here: N is the number of modes; q^n is the normalized amplitude of the mode n defined by the local energy spectrum; k^n is the amplitude of the wave number vector of the mode n , $\mathbf{k}^n = k^n \mathbf{d}^n$ (where \mathbf{d}^n is a random unit vector of direction uniformly distributed over a sphere); σ^n is a unit vector normal to \mathbf{d}^n ($\sigma^n \cdot \mathbf{d}^n = 0$) [26], and in turn the angle defining its direction in the plane normal to \mathbf{d}^n is a random number uniformly distributed in the interval $[0, 2\pi]$; φ^n is the phase of the mode n , which is also a random number uniformly distributed in the interval $[0, 2\pi]$. All these random distributions are versus n .

All the random numbers involved in Eq. 4 are defined only once, that is, they are not changed in time. To introduce the time-dependence of the fluctuations we employ a so-called “wave convection” approach, which is somewhat different from the way of imposing

⁴For linear RANS models, the normal stresses are usually set equal to 2/3 of the turbulent kinetic energy k (if k is not available from RANS, e.g., for the Spalart-Allmaras model [38], it can be approximated by $\nu_t S/0.3$).

Fig. 3 Energy spectrum used in STG



unsteadiness of the fluctuations in the original STG formulation [4]. Namely, we define the pseudo-position vector \mathbf{r}' in Eq. 4 as

$$\mathbf{r}' = \{x', y', z'\}, \quad x' = \frac{2\pi}{k^n \max\{l_e(\mathbf{r})\}} (x - U_0 t), \quad y' = y, \quad z' = z, \quad (5)$$

where U_0 is a macro-scale velocity at the RANS-LES interface (e.g., the maximum or bulk velocity),⁵ l_e is the local scale of the most energy-containing eddies (see below), and $\max\{l_e(\mathbf{r})\}$ is its maximum value over the interface.

The normalized amplitudes of the modes q^n in Eq. 4 are defined as:

$$q^n = \frac{E(k^n) \Delta k^n}{\sum_{n=1}^N E(k^n) \Delta k^n}, \quad \sum_{n=1}^N q^n = 1, \quad (6)$$

where $E(k^n)$ is a prescribed spatial spectrum of the kinetic energy of turbulence represented by a modified von Karman spectrum, shown in Fig. 3 and defined by the formula:

$$E(k) = \frac{(k/k_e)^4}{[1 + 2.4(k/k_e)^2]^{17/6}} f_\eta f_{cut}. \quad (7)$$

Here k_e is the wave number corresponding to the spectral maximum, and f_η and f_{cut} are empirical functions.

The wave number k_e in Eq. 7 corresponds to the wavelength of the most energy-containing mode, $l_e = l_e(\mathbf{r})$, of the synthetic velocity fluctuations ($k_e = 2\pi/l_e$) or, in other words, to the size of the most energy-containing eddies. A proper definition of the quantity l_e is of crucial importance to obtain a synthetic fluctuating velocity field that will rapidly evolve to the physically realistic one. In the present work we assume that it should be proportional to the RANS length-scale but, based on simple geometrical considerations, should not be larger than double the distance to the wall:

$$l_e = \min(2d_w, C_l l_t). \quad (8)$$

Here d_w is the distance of the field point to the wall, $C_l = 3.0$ is an empirical constant which was adjusted based on preliminary simulations of a plane mixing layer, and l_t is the length-scale of the background RANS model (e. g., $l_t = k_t^{1/2}/(C_\mu \omega_t)$ for the $k - \omega$ model) computed based on the steady RANS solution that is used as an initial field in RANS-LES computations.

In the near-wall part of the boundary layer (8) makes l_e equal to double the distance to the wall, whereas in its outer part l_e is proportional to the RANS length-scale. Examples of

⁵Note that the definition of a proper unique single value of U_0 in complex 3D aerodynamic flows, e.g., in a flow past a swept wing, is problematic but accumulated experience suggests that the effect of its choice is not significant.

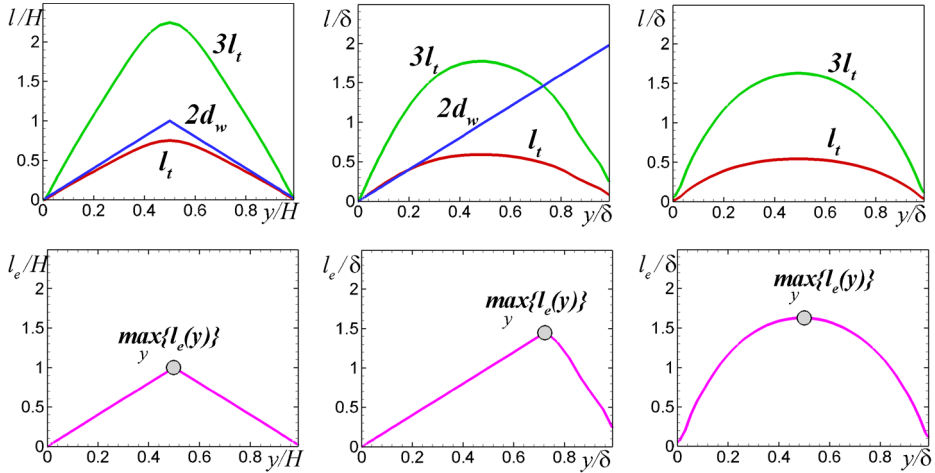


Fig. 4 Profiles of ingredients of length-scale l_e (8) (upper row) and its distribution in different shear flows (lower row). First column: plane channel; second column: ZPG BL; third column: free shear layer

normalized distributions of $l_e(\mathbf{r})$ in canonical turbulent shear flows computed with the use of the $k - \omega$ SST model [39] are presented in Fig. 4. They confirm the qualitatively correct behavior of l_e in the sense that the size of the most energetic synthetic eddies is small near the walls and the outer edge of turbulent region, and reaches a maximum value of the order of the shear layer thickness inside it.

The empirical functions f_η and f_{cut} in the energy spectrum (7) are defined as follows.

The first function is aimed at ensuring the damping of the spectrum in the vicinity of the wave number corresponding to the Kolmogorov length-scale $l_\eta = (v^3/\epsilon)^{1/4}$, i.e., $k_\eta = 2\pi/l_\eta$ (v is the molecular viscosity, ϵ is the turbulence dissipation rate). This function is designed based on the classic experiments of Comte-Bellot and Corrsin [40] and reads as:

$$f_\eta = \exp \left[- (12k/k_\eta)^2 \right]. \quad (9)$$

The function f_{cut} damps the spectrum at wave numbers larger than the Nyquist value, k_{cut} , and reads as

$$f_{cut} = \exp \left(- \left[\frac{4 \max(k - 0.9k_{cut}, 0)}{k_{cut}} \right]^3 \right), \quad k_{cut} = 2\pi/l_{cut}, \quad (10)$$

where

$$l_{cut} = 2 \min \{ [\max(h_y, h_z, 0.3h_{\max}) + 0.1d_w], h_{\max} \}, \quad (11)$$

h_y, h_z are the local grid steps at the RANS-LES interface, and $h_{\max} = \max(h_x, h_y, h_z)$.

The set of wave numbers used in Eq. 4 is fixed, i.e., it is common for the entire RANS-LES interface, and, as proposed in [36], forms a geometric series, which allows a considerable decrease of the number of modes compared with a uniform distribution of wave numbers

$$k^n = k^{\min} (1 + \alpha)^{n-1}, \quad n = 1, 2, \dots, N; \quad 0.01 \leq \alpha \leq 0.05. \quad (12)$$

Here $k^{\min} = \beta k_e^{\min}$ is the minimum wave number in the set, $\beta = 0.5$ is an empirical constant, $k_e^{\min} = 2\pi/l_e^{\max}$ is the wave number corresponding to the maximum value of l_e over the interface, $l_e^{\max} = \max_{\mathbf{r}} \{l_e(\mathbf{r})\}$, and the value of N (the number of modes in Eq. 4)

is the minimum integer, for which k^N satisfies the inequality $k^N \geq k_{\max} = 1.5 \max \{k_{cut}(\mathbf{r})\}$. Note, that, e.g., in a RANS-IDDES simulation of the ZPG BL with $\alpha = 0.01$ (see below), this definition leads to the value $N = 405$, whereas a uniform wave number distribution with the step equal to the minimum step of the geometric series would require $N \approx 5600$ modes.

Finally, if LES is performed with the use of a differential subgrid model, as in DES, some boundary conditions for the subgrid turbulence characteristics should be specified at the interface. Specifically, for LES or WMLES/IDDES with the SA or $k-\omega$ SST background models, these conditions are as follows. The SGS eddy viscosity is computed with the use of an algebraic SGS model (e.g., the Smagorinsky model for LES or the algebraic hybrid model [3] for WMLES). Then, for the SST model, the field of ω_{SGS} at the LES inflow is set equal to ω_{RANS} at this boundary, and k_{SGS} is computed to match ω_{SGS} and v_{SGS} . Although this approach is rather crude, it does not cause any tangible deterioration of the LES solutions (see next section).

To summarize, the most important distinguishing features of the STG method outlined above are as follows.

The method employs a set of wave numbers $\{k^n\}$, which is *fixed* in time and over the entire RANS-LES interface and ranges from the value corresponding to the largest wavelength of the considered problem up to the Nyquist limit. Other than that, the von Karman energy spectrum (7) defining the normalized amplitudes of different Fourier modes q^n in each point of the interface (see Eq. 6) has a maximum at locally defined wave numbers $k_e(r) = 2\pi/l_e(r)$, that is, it “slides” over the fixed set $\{k^n\}$ ensuring that larger wavelength modes get scaled by very small amplitudes near walls, where the length scale l_e (8) is small (see Fig. 4), while smaller wavelength modes get scaled by very small amplitudes away from walls. As a result, the lateral size of the energy containing structures created by the STG at the LES inflow turns out to be small in the inner and large in the outer flow regions. Finally, the global time scale $\tau_0 = l_e^{\max}/U_0$ involved in the wave-convection form of time-dependence for the synthetic velocity fluctuations (4) results in roughly the same streamwise size for all the vortical structures downstream of the interface. A combination of these properties of the STG ensures the formation of strongly anisotropic (elongated) eddies near walls, and nearly isotropic eddies away from walls.

One more important feature of the STG is that all the random quantities entering Eq. 4 are defined only once, at the beginning of the simulation (i.e., there are no random changes of phase, like in some other STG’s). With the fixed set of wave numbers for the entire RANS-LES interface, this prevents the generation of unviable high-frequency “hash” which can lead to “near-laminarization” (damping of the synthetic turbulence) downstream of the interface. Note that an alternative way of suppressing this undesirable effect within the STG [28] has been proposed recently by Batten et al. [41], but it seems to be more complicated and less efficient than the current approach.

An example of the synthetic turbulence field generated on the basis of the $k-\omega$ SST RANS in a channel flow with the use of the STG we just described and its comparison with the field from an LES of this flow carried out with periodic conditions in the streamwise direction is shown in Fig. 5. One can see that at least qualitatively the synthetic and “real” (LES-predicted) fields are quite similar.

3.1.2 Validation

The STG was validated on both incompressible canonical shear flows (developed channel flow, ZPG BL, and free plane shear layer) and on more complex flows, including

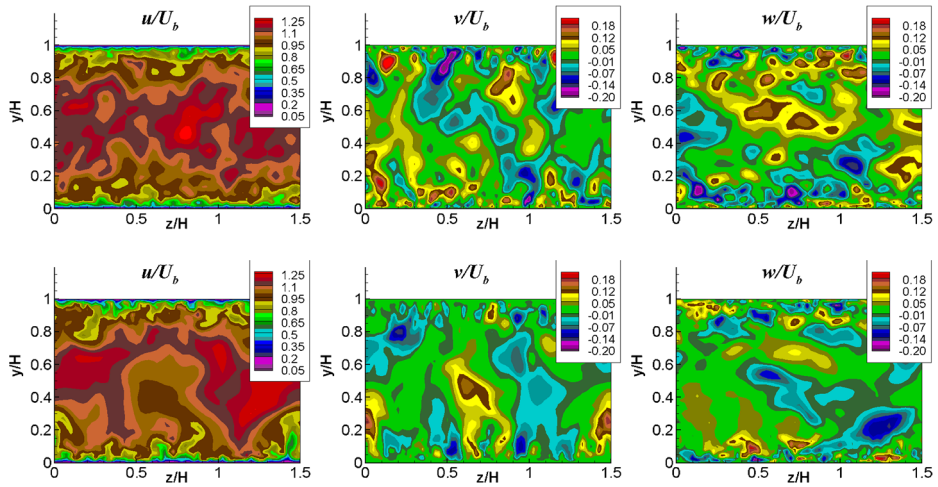


Fig. 5 Synthetic velocity field in a section of developed channel flow generated with the use of STG (*upper row*) and obtained in LES with periodic streamwise boundary conditions (*lower row*)

separation and reattachment. In this section some results of the validation are presented and discussed.

All the computations are carried out with the use of the in-house NTS CFD code [42, 43]. It is a structured finite-volume code accepting multi-block overset grids of Chimera type. The incompressible branch of the code employs the Rogers-Kwak scheme [44] and for compressible flows the Roe scheme [45] is applied. The viscous terms are approximated with second-order central differences, whereas the spatial approximation of the inviscid fluxes is different in the RANS and LES zones. In particular, in the RANS zone a 3rd-order upwind-biased scheme is used, and in the LES zone a 4th-order central scheme is employed. For the time integration, implicit 2nd-order backward Euler scheme with sub-iterations is used (a typical number of sub-iterations, ensuring 2 orders of magnitudes drop of the residuals, is 10-12).

Developed channel flow Simulations were carried out at a Reynolds number, based on the channel half width $H/2$, $\text{Re}_\tau = 400$ in a computational domain with the size $L_x = 4H$ in the streamwise and $L_z = 1.5H$ in the spanwise (homogeneous) directions respectively on a grid $N_x \times N_y \times N_z = 81 \times 77 \times 61$ which is uniform in x and z ($\Delta x = 0.05H$, $\Delta z = 0.25H$) and clustering to the wall in the wall-normal direction ($\Delta y_{\min} = 0.001H$, $\Delta y_{\max} = 0.04H$). The corresponding grid steps in wall units are $\Delta x^+ = 40$, $\Delta z^+ = 20$, and $\Delta y_{\min}^+ = 0.8$. Note that in accordance with the IDDES concept [3], the switch of the model from RANS mode to LES mode in the wall-normal direction occurs within the range of wall-distance from $0.5\Delta_{\max}$ to Δ_{\max} , where Δ_{\max} is the maximum local grid-spacing, which was equal to Δ_x in this and all the other flows considered below.

Figures 6, 7 compare results of two simulations. The first one is a non-zonal IDDES [3] based on the $k-\omega$ SST RANS model [39], carried out with periodic boundary conditions in the streamwise direction. In terms of the quality of the inlet turbulent content, this simulation may be considered as a “standard” one. The second simulation is a zonal RANS-IDDES, both RANS and IDDES employing the $k-\omega$ SST model, and the boundary conditions at the RANS-IDDES interface ($x = 0$) are specified with the use of the STG.

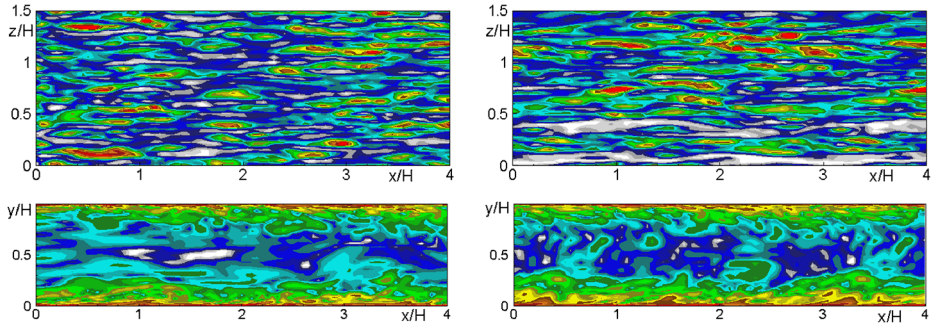


Fig. 6 Snapshots of vorticity magnitude on the channel wall (*upper row*) and in an *XY*-plane (*lower row*) of developed channel flow. Left column: zonal SST-based RANS-IDDES with the use of STG at the RANS-IDDES interface ($x = 0$); right column: non-zonal SST-based IDDES with periodic boundary conditions

Thus, the comparison of results of the two simulations allows an objective visual evaluation of the performance of the STG.

Figure 6 again suggests that the STG indeed reproduces realistic vortical structures, which are quite similar to those predicted by the IDDES with periodic boundary conditions. In quantitative terms, the mean skin-friction distribution predicted by the zonal RANS-IDDES also turns out to be very close to that computed with the use of the non-zonal IDDES, and has a very short adaptation region (Fig. 7). Moreover, as seen in Fig. 7, not only the mean velocity but also the Reynolds-stress profiles from the zonal RANS-IDDES agree fairly well with the corresponding profiles predicted by the non-zonal IDDES already at $x = 2H$ (i.e., 4 boundary layer thicknesses downstream of the RANS-IDDES interface) and correctly reproduce the anisotropy of the normal stresses, even though the synthetic turbulence at the interface is computed based on a linear RANS model, i.e., it has identical normal stresses. Other than that, a comparison of the zonal simulations carried out with the use of the proposed STG and another synthetic method (SEM [22]) is also shown in Fig. 7, and the former achieves a much shorter adaptation length and higher global accuracy than the latter.

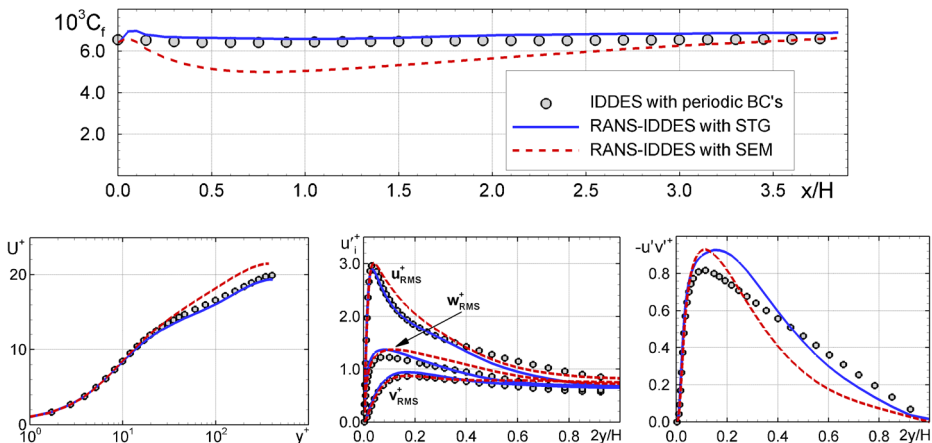


Fig. 7 Comparison of streamwise distributions of skin-friction coefficient and profiles of the mean velocity and Reynolds stresses in wall units at $x = H$ from non-zonal IDDES and zonal RANS-IDDES

Finally, it should be noted that with the restricted length of the computational domain used in the simulations ($L_x = 4H$), the zonal RANS-IDDES with the STG, in a sense, surpasses the non-zonal IDDES with the periodic boundary conditions. In particular, unlike the former, the latter reveals a very large streamwise correlation length, close to L_x (see Fig. 6) and also unnatural peaks in the velocity spectra (not shown) at the frequency corresponding to the flow-through time and its multiples, which are directly related to the assumption of streamwise periodicity of the flow.

Zero pressure gradient boundary layer Simulations of this flow were performed with momentum thickness Reynolds number $Re_{\theta_0} = 1000$ in a computational domain with the size $L_x = 25\delta_0$, $L_y = 10\delta_0$, and $L_z = 3\delta_0$ in the streamwise, wall-normal, and spanwise directions respectively. The grid $N_x \times N_y \times N_z = 251 \times 71 \times 61$ was again uniform in the x - and z -directions ($\Delta_x = 0.1\delta_0$, $\Delta_z = 0.05\delta_0$) and non-uniform (clustering near the wall) in the wall-normal direction with $\Delta y_{\min} = 0.0025\delta_0$. The corresponding steps in wall units are not larger than $\Delta x^+ = 40$, $\Delta z^+ = 20$, and $\Delta y_{\min}^+ = 1.0$. Results of these simulations are presented in Figs. 8, 9, 10, 11. They compare a prediction of the $k-\omega$ SST IDDES carried out with the use of a recycling procedure [9] (the length of the recycling region being equal to $6\delta_0$) with similar predictions of the zonal RANS-IDDES coupled with the STG and, also, with the DNS results of Spalart [46] as a benchmark solution.

Figures 8, 9 clearly illustrate the advantages of the STG method over the recycling approach in terms of representation of turbulence. In particular, as seen in Fig. 8, although both methods ensure a rapid formation of realistic turbulence in the inner (near wall) region of the boundary layer, away from the wall the recycling of turbulence leads to the formation of non-physical periodic structures (they are marked by ovals in the figure) with a period close to the recycling length. This behavior of the recycling approach is similar to that discussed above regarding the channel flow with imposed streamwise periodicity and, as mentioned, is especially troublesome in aeroacoustic applications. This deficiency is clearly demonstrated also by Fig. 9: as seen in this figure, the STG method ensures a rapid establishment of the “natural” spectrum of the velocity fluctuations with a pronounced inertial range (the decay follows the “-5/3” law), whereas the recycling of turbulence leads to spurious spectral peaks at multiples of the main recycling frequency, which originate in the periodic vortical structures displayed in Fig. 8. Although this negative effect can be weakened by increasing the recycling length, it still remains significant if using reasonable values for that length. In addition, longer recycling lengths increase waste, and also increase the unwanted secondary effects of recycling. Specifically, in boundary layers, the growth of the thickness

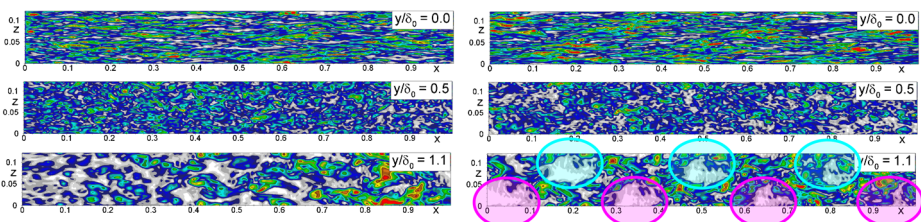


Fig. 8 Snapshots of vorticity magnitude in different XZ planes of ZPG BL. *Left column* zonal RANS-IDDES with STG; *right column* IDDES with turbulence recycling

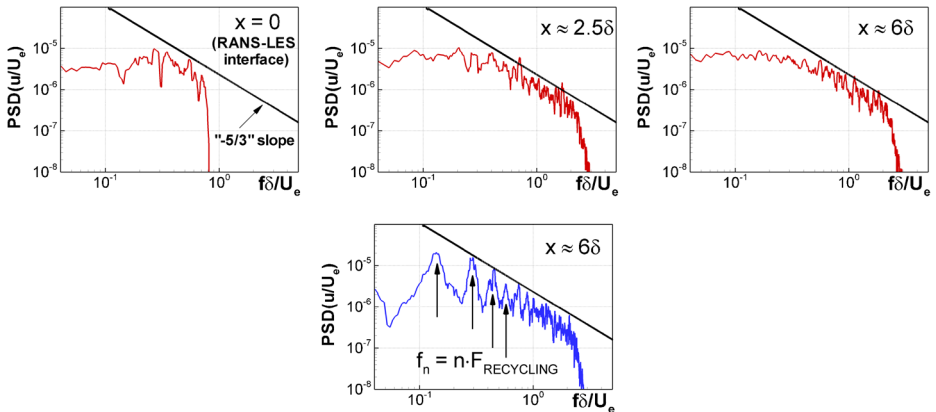


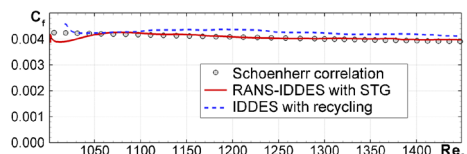
Fig. 9 Streamwise evolution of the spectrum of velocity fluctuation in the *middle* of the BL ($y/\delta \approx 0.5$) from zonal RANS-IDDES with STG (*upper row*), and spectrum from IDDES with turbulence recycling

is compensated as part of the recycling, but the growth of the lateral length scales and of the temporal scales is not. Therefore, with a long recycling length, the recycled turbulence is less natural, and will have a slightly longer adaptation region.

Figures 10, 11 compare streamwise distributions of the skin-friction, C_f , and velocity and Reynolds stress profiles predicted by the two simulations. They show that both approaches predict C_f distributions close to each other and to the empirical Schoenherr correlation [47]. At the same time, close to the interface the mean velocity profiles from the zonal RANS-IDDES with the STG deviate somewhat from the DNS profiles and those predicted with the use of the recycling procedure (Fig. 11). This, however, is explained not by any flaws of the STG itself, but by an imperfection of the RANS solution it is based on. The latter is caused by the relatively low Reynolds number of the flow, at which the RANS models are known to be less accurate, and also by not accounting fully for the anisotropy of the Reynolds stresses in the linear $k-\omega$ SST model. This is clearly seen in the plots of the Reynolds stresses at the RANS-IDDES interface ($x=0$) in Fig. 11: the recycling approach captures the anisotropy fairly well, whereas the STG method, naturally, completely misses it there (this would be alleviated by a non-linear constitutive relation). Nonetheless, just as in the developed channel flow considered above, the recovery of the anisotropy in the IDDES domain within the RANS-IDDES approach occurs rapidly, and already at $x/\delta=3$ the normal stresses predicted by both approaches have become comparable.

Plane mixing layer This flow, studied experimentally in [48], is the last canonical shear flow used for the validation of the proposed STG. As for the previous flows, the computations were carried out with the use of the zonal RANS-IDDES based on the $k-\omega$ SST RANS model. However in this case three different locations of the RANS-IDDES interface were

Fig. 10 Streamwise distributions of skin friction coefficient in ZPG BL



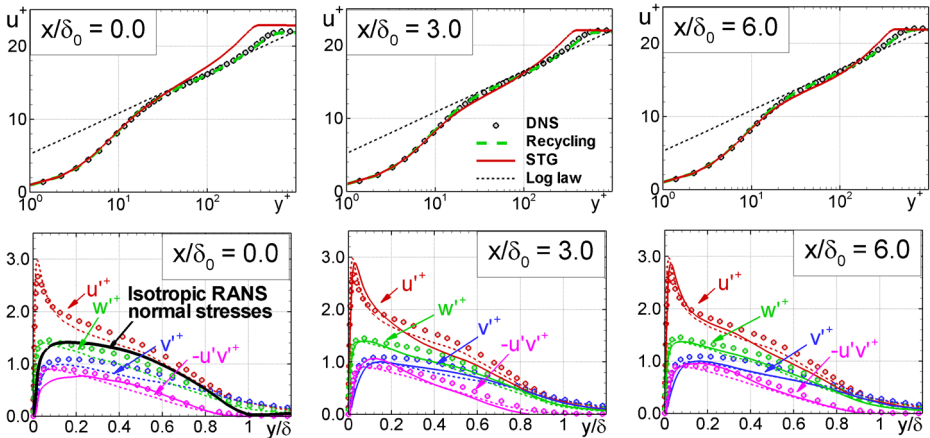


Fig. 11 Streamwise evolution of profiles of mean velocity and Reynolds stresses. Symbols DNS [46]; dashed lines SST-based IDDES with recycling; solid lines RANS-IDDES with STG

used (see Fig. 12). The corresponding IDDES sub-domains have the following dimensions: $0.2m \leq x \leq 0.6m$, $-0.8m \leq y \leq 0.8m$, $0 \leq z \leq 0.08m$ (domain 1); $0.5m \leq x \leq 1.5m$, $-1.0m \leq y \leq 1.0m$, $0 \leq z \leq 0.18m$ (domain 2); $1.0m \leq x \leq 2.3m$, $-1.2m \leq y \leq 1.2m$, $0 \leq z \leq 0.28m$ (domain 3). The vorticity thickness of the shear layer varies from about $0.013m$ at $x = 0.2m$ up to $0.12m$ at $x = 2.3m$, and the streamwise grid step varies from $9.8 \cdot 10^{-4}m$ up to $9.8 \cdot 10^{-3}m$. The grid in the spanwise direction is uniform with a step around 0.0033 of the maximum vorticity thickness in the corresponding sub-domain, $\delta_{\omega_{\max}}$. Finally, the minimum transverse grid-step, Δy_{\min} , in each sub-domain is around $0.01\delta_{\omega_{\max}}$.

Figure 13 presents instantaneous vorticity fields in the IDDES sub-domains from these three simulations and the whole field obtained by pasting the separate fields together, and Fig. 14 compares the mean flow characteristics predicted by the RANS-IDDES with those of SST RANS and experimental data. The figures do not reveal any visible discontinuities at the three RANS-IDDES interfaces, and suggest that for the considered flow the STG ensures a very good agreement with experimental data.

Thus, the results of testing the STG in canonical shear flows (both wall-bounded and free) are rather encouraging and justify the application of the method to more complex generic flows. Two examples of such flows are considered below.

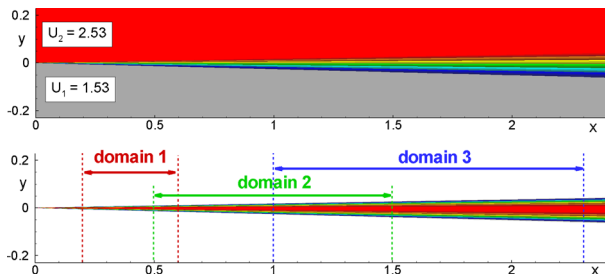


Fig. 12 Contours of the streamwise velocity (upper frame) and vorticity magnitude (lower frame) in the plane shear layer predicted by $k-\omega$ SST RANS. Lower frame shows also IDDES sub-domains in three RANS-IDDES simulations

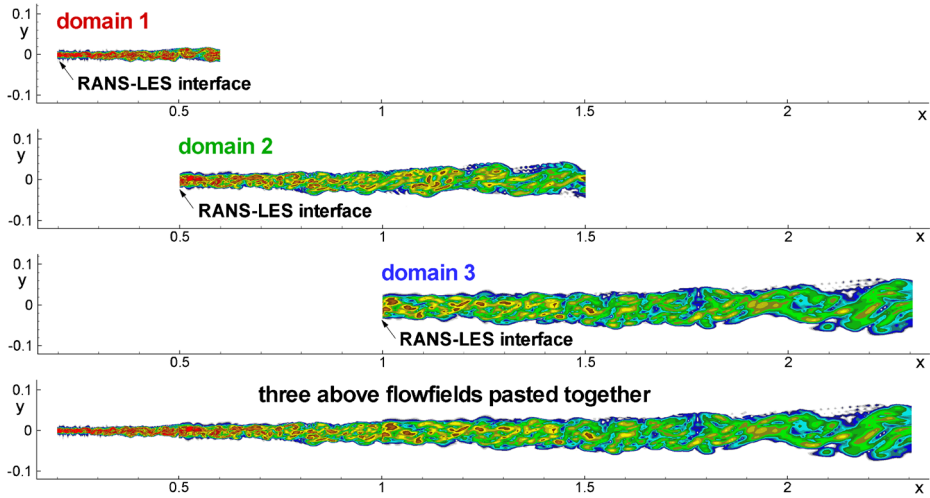


Fig. 13 Instantaneous vorticity fields in the plane shear layer from RANS-IDDES with different locations of the RANS-IDDES interface

Flow past a wall-mounted hump This flow (see schematic in Fig. 15) was studied in experiments [49], and the accurate prediction of its major physical features (non-fixed separation, reattachment and recovery of the reattached boundary layer) is a serious challenge for any RANS model, which has made the flow a valuable test case for different approaches to turbulence representation. Figure 15 shows also the computational domain with overlapping RANS and IDDES sub-domains used in the zonal RANS-IDDES of the flow (the span size of the domain was $0.4c$). Along with this simulation, global RANS and IDDES were carried out.

Simulations were performed on a grid with $N_x \times N_y \times N_z = 379 \times 111 \times 101$ nodes. The grid is strongly refined in the x -direction in the vicinity of the hump and downstream

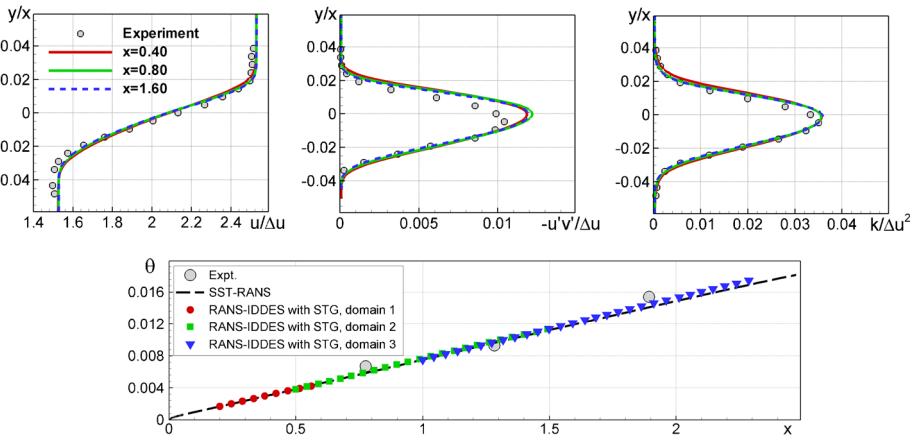


Fig. 14 Streamwise variation of the mean velocity, total (resolved plus modelled) shear stress, and turbulent kinetic energy (upper row) and momentum thickness (lower frame) in the plane shear layer

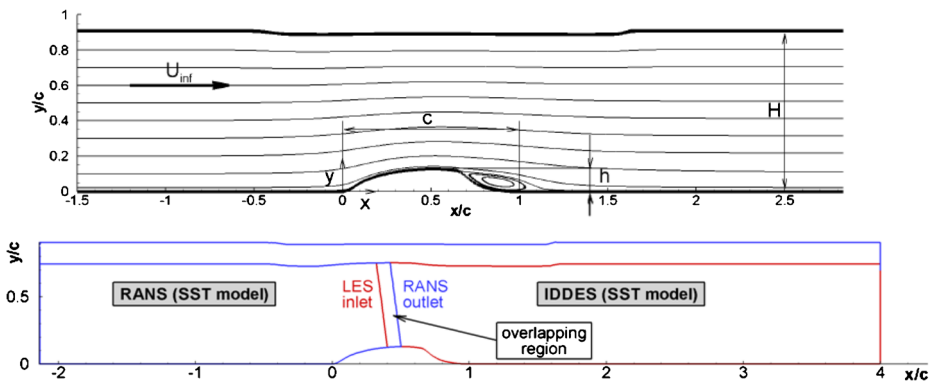


Fig. 15 Schematic of wall-mounted hump flow [49] and computational domain with overlapping RANS and IDDES sub-domains

of the separation region, where the x -step is set equal to $0.005c$, and then is gradually coarsening up to the maximum value of $0.05c$. The wall-normal grid is clustering near the wall ($\Delta y_1 = 1.5 \cdot 10^{-5}c$) and is kept fine (Δy is no larger than $0.005c$) in the recirculation zone and in the separated shear layer. As a result, the grid in this region is nearly isotropic. Finally, the ranges of the grid-steps in the law of the wall units are as follows: $y_1^+ < 0.7$, $300 < \Delta x^+ < 3000$, and Δz^+ is around 250.

Figures 16, 17 present some results of the simulations. In particular, Fig. 16 compares flow visualization from the pure IDDES (with RANS incoming boundary-layer treatment and autonomous switch to LES mode after separation) with that from a zonal RANS-IDDES simulation with the interface located at $x/c = 0.4$. A striking difference of the two flow patterns is that according to the IDDES in the whole domain the initial region of the shear layer separated from the hump remains nearly 2D, whereas the zonal RANS-IDDES, due to the presence of the turbulent content created by the STG at the IDDES inlet, predicts a rapid formation of 3D chaotic vortical structures. As a result, the prediction of the mean flow characteristics in the initial part of the separation bubble by the pure IDDES turns out to be even less accurate than that of the pure RANS, whereas the zonal RANS-IDDES ensures a close agreement with the data in the whole domain. This is clearly seen from comparison of the mean skin-friction distributions predicted with the use of the three approaches with

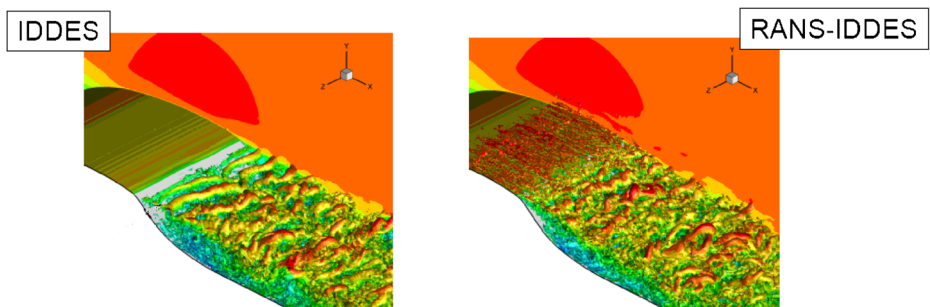


Fig. 16 Flow visualizations (isosurface of “swirl” coloured by streamwise velocity magnitude) from pure SST-based IDDES and zonal SST RANS-IDDES with STG at the interface

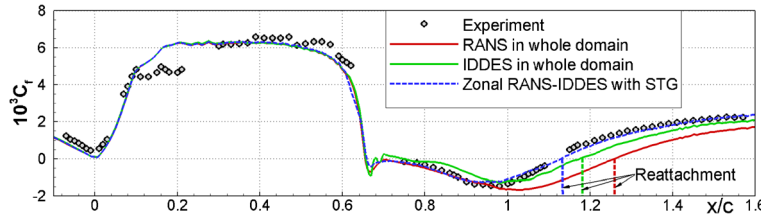


Fig. 17 Comparison of computed streamwise distributions of skin-friction with experiment

the experiment shown in Fig. 17 (the mean flow characteristics were computed by time- and z-averaging of the solution over 30 convective time units, c/U_{inf} , after nearly the same transient period).

To summarize, as far as aerodynamic flow characteristics are concerned, the STG described above offers a tool which is not only rather simple and robust but, also, fairly accurate for creating turbulent content within zonal RANS-(WM)LES approaches. However, the experience of its application “as is” to airframe noise prediction suggests that in this case it leads to unacceptable results. This is illustrated by Fig. 18, where acoustic and turbulence fields are presented from the RANS-IDDES computations of the airfoil trailing edge test case considered within the EC Project VALIANT [50] (see [51] for details). For this flow the dominant real noise source is known to be located in the trailing edge region. However, in this simulation, the acoustic field turns out to be overwhelmed by the strong waves (“spurious noise”) generated at the RANS-IDDES interface by abruptly emerging strong vortical structures created there by the STG (as noted earlier, this is not a unique feature of the considered STG, but an inherent property of any known STG). Thus, some modifications aimed

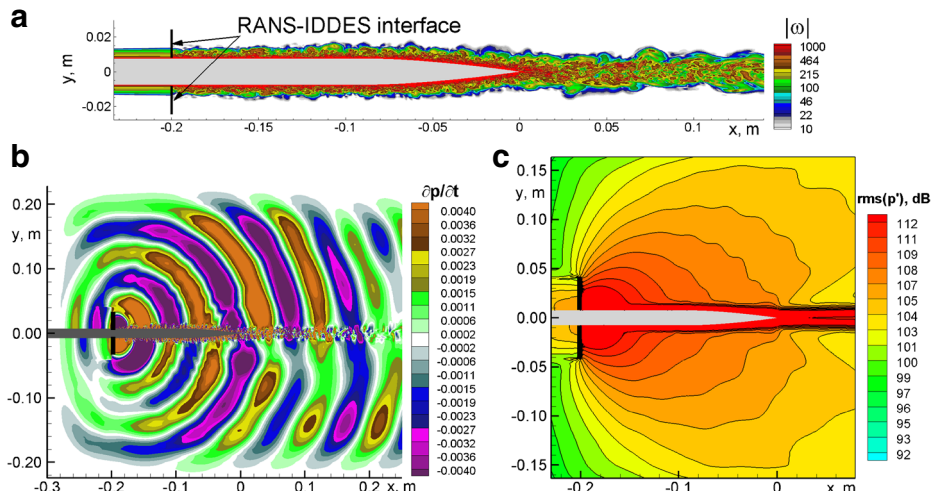
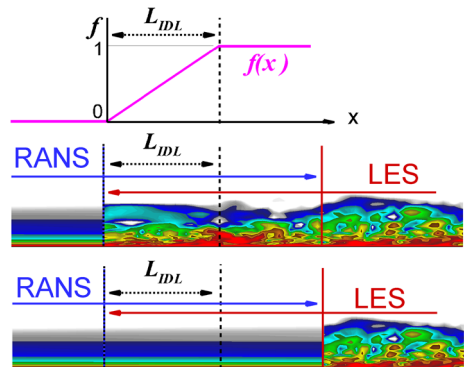


Fig. 18 Instantaneous vorticity (a), acoustic pressure time-derivative contours (b), and $rms(p')$ of pressure fluctuations (c) for $M=0.15$ trailing edge flow [51] obtained by from zonal RANS-IDDES with the use of the STG

Fig. 19 Design of internal damping layer



at suppressing this spurious noise without damaging the real noise generated by the flow are highly necessary in order to make the STG applicable to aero-acoustic problems. Such a modification is outlined in the next section.

3.2 “Acoustically adapted” STG formulation and testing on trailing edge flow

The proposed way of suppressing the spurious noise created by synthetic turbulence at the RANS-LES interface consists in inserting an “internal damping layer” (IDL) in the LES

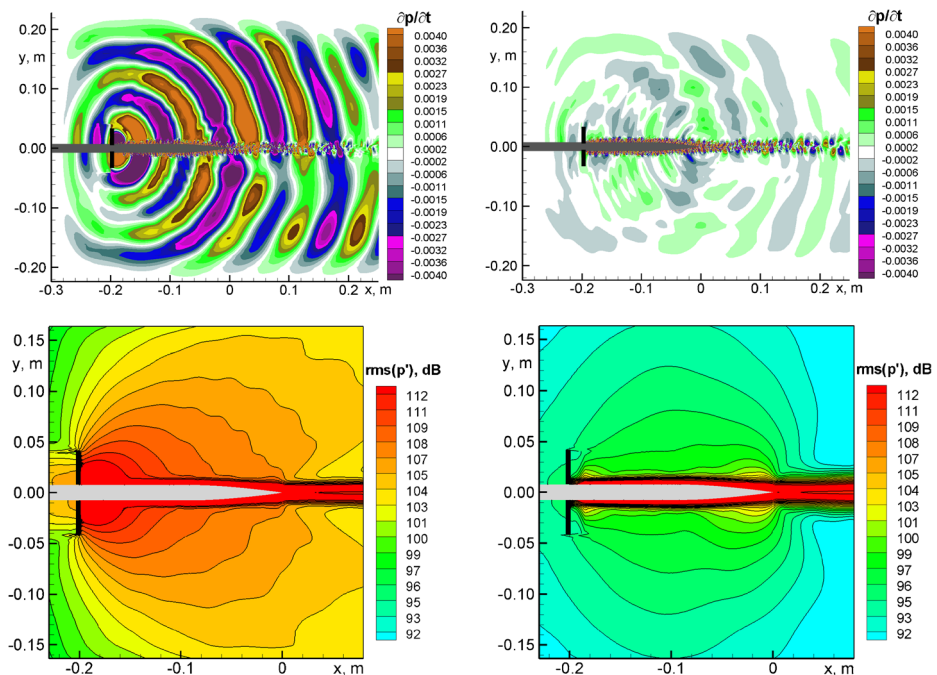


Fig. 20 Instantaneous acoustic pressure (upper row) and *rms* of pressure fluctuations (lower row). Left column original STG; right column STG with internal damping layer

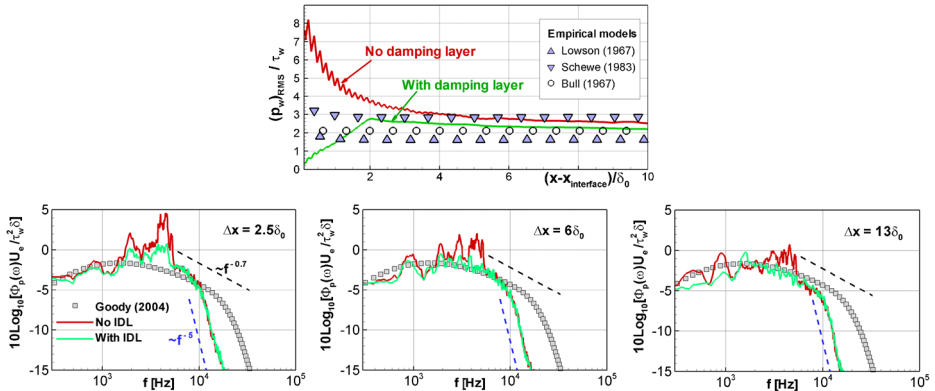


Fig. 21 Effect of internal damping layer on *rms* of wall-pressure fluctuations in IDDES sub-domain of RANS-IDDES (upper frame) and on power spectra of wall pressure. Empirical correlations shown by symbols are from [52–55]

sub-domain of the zonal RANS-LES. The idea and design of the damping layer is clarified by Fig. 19.

The IDL is placed within the overlapping region of the RANS and LES sub-domains, and inside this layer at each time step a “preliminary” (computed by LES) pressure field is modified by “weighting” it with the URANS pressure, also available in the overlapping region:

$$p_{LES}^{\text{mod}} = f(x) \cdot p_{LES} + [1 - f(x)] \cdot p_{RANS},$$

where the empirical weight function $f(x)$ is defined as $f = \max \{ \min [(x - x_0) / L_{IDL}, 1], 0 \}$, x_0 is the streamwise coordinate of the IDDES inlet, and L_{IDL} is the damping layer length (typically, it is set equal to $\sim 2\delta_{BL}$, which is rather short).⁶ The velocity and temperature fields within the IDL region remain unchanged, and the density is re-computed with the use of the modified pressure to match the equation of state.

The drastic positive effect of this simple modification is illustrated by Fig. 20 which compares the acoustic pressure field and *rms* of the pressure fluctuations predicted with the use of the original (purely aerodynamic) and the modified versions of the STG within the $k-\omega$ SST based zonal RANS-IDDES. One can see, in particular, that the damping layer results in a radical weakening, if not a complete eliminating of the spurious sound source at the RANS-IDDES interface and makes the real sound source located near the sharp trailing edge the dominating one. Note also that although the real noise sources within the damping layer are significantly damped, the intensity of the wall pressure fluctuations in this region predicted by the original STG (without the damping layer) is strongly overestimated, and, as seen in Fig. 21 (upper frame), in this respect the STG with damping layer not only does not result in any additional inaccuracy, but turns out to be even somewhat more accurate than the purely aerodynamic STG version. The same is true regarding the spectral characteristics of the unsteady wall-pressure in the IDDES sub-domain, even right downstream of the damping layer: as seen in the right frame of Fig. 21, the damping layer ensures a much

⁶An alternative method for suppression of the spurious noise at the RANS-LES interface based on the sponge layer technique (introduction of appropriate volume sources in the governing equations) was proposed by Roidl et al. [34, 35].

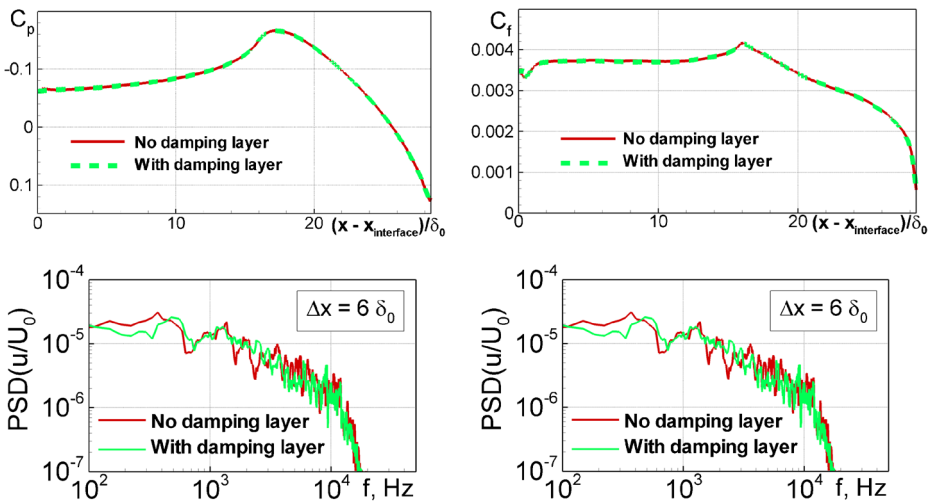


Fig. 22 Effect of internal damping layer on mean wall pressure and friction coefficients and on spectra of velocity fluctuations in the middle of boundary layer ($y/\delta \approx 0.5$)

better agreement with an empirical correlation [55]. Finally, it should be emphasized that the damping layer does not preclude the capture of sound waves generated by noise sources located downstream of the end of the RANS sub-domain and propagating upstream (within the damping layer, they propagate through the RANS area).

Thus, in terms of acoustics, the trailing edge test case does not reveal any negative secondary effects of the proposed acoustically adapted STG. The same conclusion can be drawn regarding the mean flow characteristics and velocity spectra: as seen in Fig. 22, at least at the present low Mach number, the damping layer does not cause any noticeable alteration of their prediction.

3.3 Application of “Acoustically adapted” STG to a wing-flap configuration

The last flow used for validation of the STG developed here is the wing-flap configuration studied experimentally by Lemoine et al. [51]. In the experiments the wing is modelled by a long plate with a sharp trailing edge, and the flap is a NACA0012 airfoil. The Reynolds number based on the free-stream velocity ($U_0 = 50$ m/s) and the flap chord ($c = 0.1$ m) is $Re_{flap} = 3.3 \cdot 10^5$, and the Mach number is $M=0.15$. Two specific configurations have

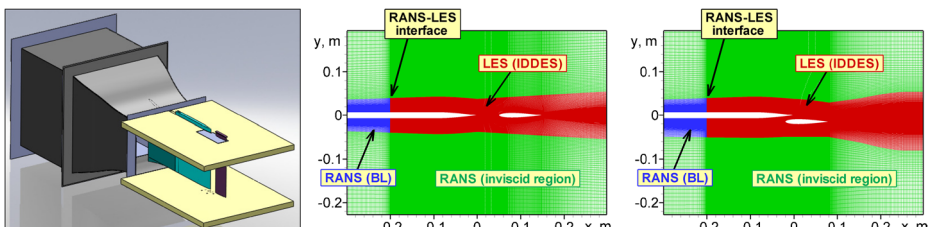


Fig. 23 Experimental setup [51] and some elements of computational grid in XY plane used in RANS-IDDES of the wing-flap flow (Configurations 2 and 4)

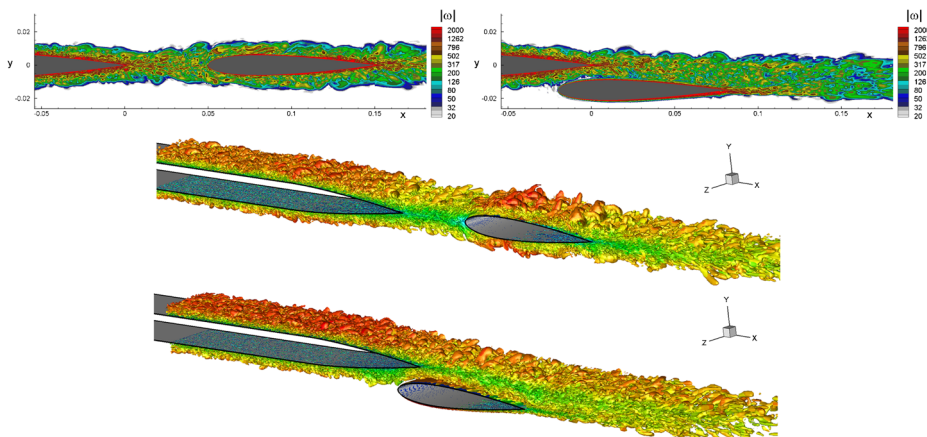


Fig. 24 Instantaneous vorticity contours (upper row) and swirl isosurfaces $\lambda = 200 U_0 / c_{flap}$ colored by streamwise velocity

been investigated with somewhat different mechanisms of noise generation: in the first one (Configuration 2, following [51]), the plate and flap are aligned, and in the second (Configuration 4), the flap is shifted down (see Fig. 23).

Just as in all the previous cases, simulations presented below are RANS-IDDES based on the $k-\omega$ SST model. The RANS-IDDES interface is located at 0.2m upstream of the plate trailing edge. The grid in the IDDES sub-domain is designed in accordance with the well-known guidelines of wall-modeled LES. Particularly, the near-wall step is 8×10^{-6} m, which ensures for the nearest distance to the wall in the law of wall units $\Delta y_1^+ < 1.2$ everywhere in the domain. The values of grid steps in the x (streamwise) direction, Δx , are less than $\delta_{BL} / 10$. In the spanwise direction the flow is assumed to be homogeneous, and periodic boundary conditions are used with a period of $L_z = 0.03$ m (1/10 of the span of the experimental model [51]). The grid in this direction is uniform and has 100 cells (this corresponds to a grid step Δz less than $\delta_{BL} / 20$). The total grid count is around 18 million cells.

Figure 24 shows typical flow visualizations from the simulations of the two configurations. It visually displays the fine-grained turbulence in the boundary layer of the main wing, and its interaction with the flap surface. Corresponding snapshots of the acoustic pressure

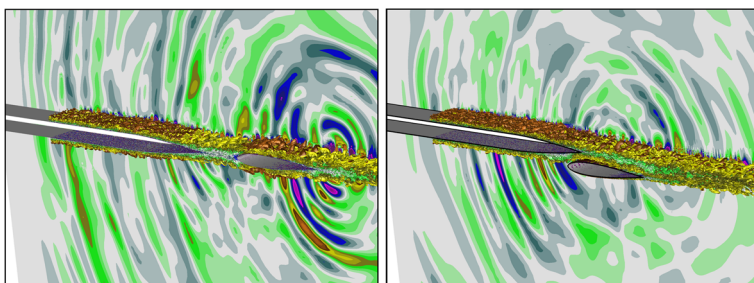


Fig. 25 Snapshots of pressure time-derivative in the acoustic range from simulations of the two considered configurations combined with instantaneous swirl isosurface

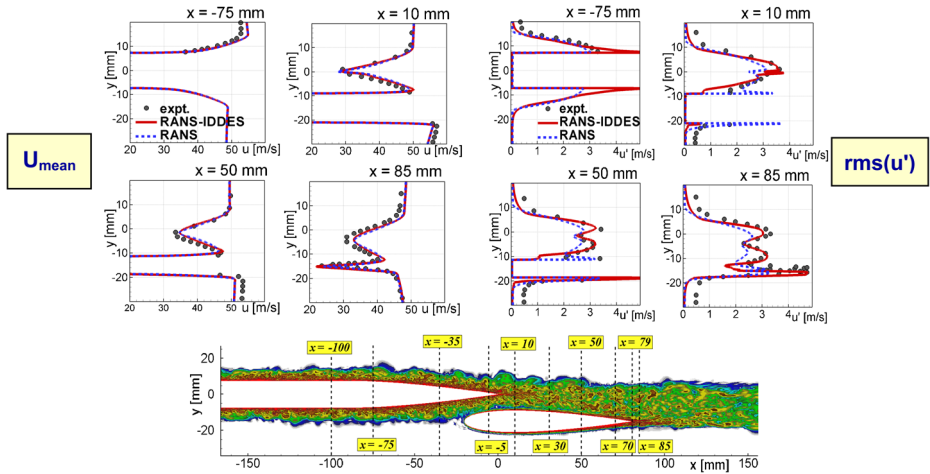


Fig. 26 Comparison of predicted and measured mean velocity and *rms* of velocity fluctuations for the wing-flap flow, Configuration 4

fields (Fig. 25) reveal different strengths and locations for the main sound sources in the two configurations (the vicinity of the flap trailing edge in the first, and the region near its leading edge in the second). Note also that neither these snapshots nor the animations of the acoustic field reveal any visible spurious sources of sound at the RANS-IDDES interface, thus confirming the efficiency of the proposed internal damping layer technique.

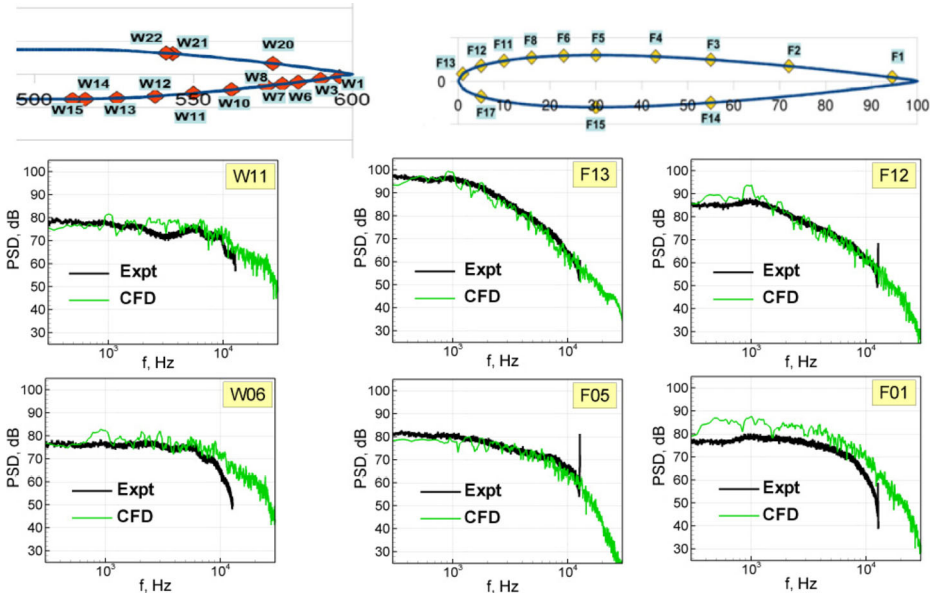


Fig. 27 Location of wall-pressure sensors on wing and flap surface in experiment [51] and comparison of RANS-IDDES predictions of wall-pressure spectra for Configuration 2 with experiment

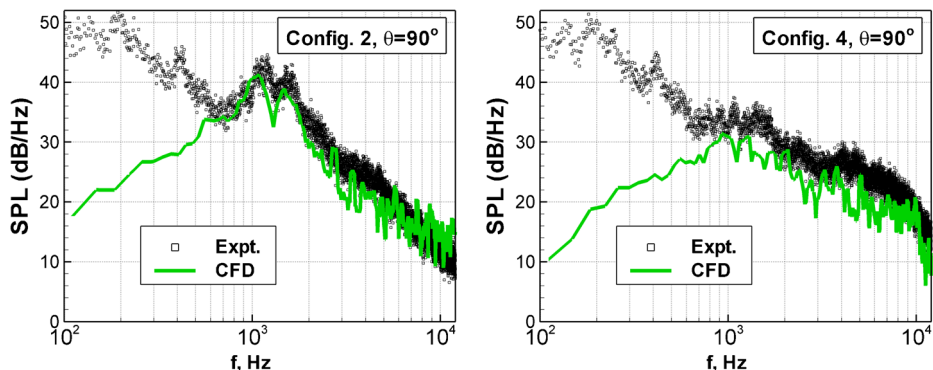


Fig. 28 Comparison of predicted and measured far-field noise spectra for Configurations 2 and 4 for an observer located at polar angle 90 degrees at a distance of 2m from the wing trailing edge

Figure 26 compares experiment, RANS and zonal RANS-IDDES predictions of the mean velocity and the intensity of its fluctuations for Configuration 4, as an example. It suggests that both approaches ensure almost equally good agreement with the data on the mean velocity profiles, which is quite natural for an attached boundary layer in the absence of strong adverse pressure gradient. In contrast to this, for the rms of the streamwise velocity fluctuation, $\text{rms}(u')$, the figure reveals a significant superiority of the RANS-IDDES over RANS (in this case, $\text{rms}(u')$ is computed as $(2/3k)^{1/2}$), except for the initial part of the lower side of the flap, where the turbulent structures populating the very thin boundary layer cannot be captured on the grid used in the simulation. Fairly good agreement of the zonal RANS-IDDES predictions with the experiment is observed also for the wall pressure spectra (see Fig. 27): the simulations correctly reproduce the variation of both the spectral shapes and levels over the main wing and flap surfaces. Some deviation of the predicted level of the fluctuations from the experimental result is observed only near the flap trailing edge (F01 sensor). The root cause of this discrepancy is not clear but it may well be caused by an inaccuracy of the experiment since it is natural to expect an increase rather than decrease of unsteadiness in this point compared to the sensor F05.

Finally, Fig. 28 compares results of computations of the far-field noise generated by the flow with measurements [51]. In order to deal with the periodicity of the simulation with a relatively narrow domain, the computations were carried out in the framework of a modification of the Ffowcs Williams and Hawkings method [56, 57] with the use of the assumption that the inputs of separate spanwise patches of length L_z into the total noise are non-correlated.⁷ The figure shows that except for the low frequency range where the measurements are probably contaminated by background wind-tunnel noise, the agreement with the data is rather good (similar agreement is observed for other polar angles).

4 Conclusions and Outlook

The paper outlines the state of the art in the problem of creating turbulent content at the RANS-(WM)LES interface in the framework of zonal LES. This is an area of intensive

⁷This assumption is supported by an analysis of the computed coherence maps of unsteady wall pressure (not shown).

research in both pure aerodynamics and aeroacoustics, and numerous approaches have been proposed. We believe it will be used extensively for research and applied simulations in the future. The paper presents the detailed formulation of a new procedure which belongs to a wide range of techniques known as synthetic turbulence generators (STG). This procedure is simple and robust and, based on the results of its extensive validation within the RANS-IDDES approach, ensures a quite acceptable accuracy for a wide range of aerodynamic and aeroacoustic problems. A primary direction for further studies should be, therefore, its systematic evaluation and wider comparison with other available approaches. Note that this in itself is a challenging task since isolating the effect of the turbulent content at the RANS-LES interface from the effects of the many other elements typically involved in complex aerodynamic and aeroacoustic computational systems is far from trivial, and its solution demands a careful design of the corresponding numerical studies.

Acknowledgments The authors from NTS gratefully acknowledge financial support of the research provided by Boeing Commercial Airplanes, the European Commission (7th Framework Programme Project VALIANT, Grant agreement ACP8-GA-2009-233680), and Russian Foundation for Basic Research (grant 12-08-00256-a).

References

1. Spalart, P.R., Jou, W., Strelets, M., Allmaras, S.: Comments on the feasibility of LES for wings, and on a hybrid RANS/LES approach. In: Liu, C., Liu, Z. (eds.) *Advances in DNS/LES*. Greyden Press, Columbus (1997)
2. Spalart, P.R., Deck, S., Shur, M.L., Squires, K.D., Strelets, M.Kh., Travin, A.: A new version of detached-eddy simulation, resistant to ambiguous grid densities. *Theor. Comput. Fluid Dyn.* **20**, 181–195 (2006)
3. Shur, M.L., Spalart, P.R., Strelets, M.Kh., Travin, A.K.: A hybrid RANS-LES approach with delayed-DES and wall-modelled LES capabilities. *Int. J. Heat Fluid Flow* **29**, 1638–1649 (2008)
4. Adamian, D.Y., Strelets, M.Kh., Travin, A.K.: An efficient method of synthetic turbulence generation at LES inflow in zonal RANS-LES approaches to computation of turbulent flows. *Math. Model.* **23**, 7, 3–19 (2011). In Russian
5. Spalart, P.R.: Detached-Eddy simulation. *Annu. Rev. Fluid Mech.* **41**, 181–202 (2009)
6. Garnier, E., Adams, N., Sagaut, P.: *Large Eddy Simulation for Compressible Flows*. Springer (2009)
7. Schlüter, J., Moin, P., Pitsch, H.: Large-eddy simulation inflow conditions for coupling with Reynolds-averaged flow solvers. *AIAA J.* **42**, 478–484 (2004)
8. Lund, T., Wu, X., Squires, K.: Generation of turbulent inflow data for spatially-developing boundary layer simulations. *J. Comput. Phys.* **140**, 233–258 (1998)
9. Spalart, P.R., Strelets, M., Travin, A.: Direct numerical simulation of large-eddy-break-up devices in a boundary layer. *Int. J. Heat and Fluid Flow* **27**, 902–910 (2006)
10. Shur, M.L., Spalart, P.R., Strelets, M.Kh., Travin, A.K.: A rapid and accurate switch from RANS to LES in boundary layers using an overlap region. *Flow, Turbul. Combust.* **86**, 179–206 (2011)
11. Araya, G., Castillo, L., Meneveau, C., Cansen, K.: A dynamic multi-scale approach for turbulent inflow boundary conditions in spatially developing flows, Vol. 670, pp. 581–605 (2011)
12. Morgan, B., Larsson, J., Kawai, S., Lele, S.K.: Improving low-frequency characteristics of recycling/rescaling inflow turbulence generation. *AIAA J.* **49**, 582–597 (2011)
13. Sagaut, P., Deck, S., Terracol, M.: *Multiscale and Multiresolution Approaches in Turbulence*. Imperial College Press (2006)
14. Keating, A., Piomelli, U., Balasas, E., Kaltenbach, H.-J.: A priori and a posteriori tests of inflow conditions for large-eddy simulation. *Phys. Fluids* **16**, 4696–4712 (2004)
15. Keating, A., De Prisco, G., Piomelli, U.: Interface conditions for hybrid RANS/LES calculations. *Int. J. Heat and Fluid Flow* **27**, 777–788 (2006)
16. Tabor, G., Baba-Ahmadi, M.: Inlet conditions for large eddy simulation: a review. *Comput. Fluids* **39**, 553–567 (2010)
17. Xie, Z.-T., Castro, I.P.: Efficient generation of inflow conditions for large eddy simulation of street-scale flows. *Flow, Turbul. Combust.* **81**, 449–470 (2008)

18. Klein, M., Sadiki, A., Janicka, J.: A digital filter based generation of inflow data for spatially developing direct numerical or large eddy simulations. *J. Comput. Phys.* **186**, 652–665 (2003)
19. Di Mare, L., Klein, M., Jones, W., Janicka, J.: Synthetic turbulence inflow conditions for large-eddy simulation. *Phys. Fluids* **18**(025107), 1–11 (2006)
20. Kornev, N., Hassel, E.: Method of random spots for generation of synthetic inhomogeneous turbulent fields with prescribed autocorrelation functions. *Commun. Numer. Methods Eng.* **23**, 35–43 (2007)
21. Veloudis, I., Yang, Z., McGuirk, J.J., Page, G.J.: Spencer, A. Novel implementation and assessment of a digital filter based approach for the generation of LES inlet conditions. *Flow, Turbul. Combust.* **79**, 1–24 (2007)
22. Jarrin, N., Benhamadouche, S., Laurence, D., Prosser, R.: A synthetic-eddy-method for generating inflow conditions for large-eddy simulations. *Int. J. Heat and Fluid Flow* **27**, 585–593 (2006)
23. Jarrin, N., Prosser, R., Uribe, J., Benhamadouche, S., Laurence, D.: Reconstruction of turbulent fluctuations for hybrid RANS/LES simulations using a synthetic-eddy method. *Int. J. Heat and Fluid Flow* **30**, 435–442 (2009)
24. Mathey, F., Cokljat, D., Bertoglio, J.-P., Sergent, E.: Assessment of the vortex method for Large Eddy Simulation inlet conditions. *Prog. Comput. Fluid Dyn.* **6**, 58–67 (2006)
25. Pamiès, M., Weiss, P.-E., Garnier, E., Deck, S., Sagaut, P.: Generation of synthetic turbulent inflow data for large eddy simulation of spatially evolving wall-bounded flows. *Phys. Fluids* **045103**, 21 (2009)
26. Kraichnan, R.: Diffusion by a random velocity field. *Phys. Fluids* **13**, 22–31 (1970)
27. Smirnov, A., Shi, S., Celik, I.: Random flow generation technique for Large Eddy Simulations and Particle-Dynamics Modeling. *J. Fluids Eng.* **123**, 359–371 (2001)
28. Batten, P., Goldberg, U., Chakravarthy, S.: Interfacing statistical turbulence closures with large-eddy simulation. *AIAA J.* **42**, 485–492 (2004)
29. Huang, S., Li, Q., Wu, J.: A general inflow turbulence generator for large eddy simulation. *J. Wind Eng. Ind. Aerodyn.* **98**, 600–617 (2010)
30. Gritskevich, M.S., Garbaruk, A.V.: Embedded LES with the use of volume source to create turbulent fluctuations. *Nauchno-technicheskie vedomosti SPbSPU* **141**, 27–36 (2012). In Russian
31. Spille-Kohoff, A., Kaltenbach, H.-J.: Generation of turbulent inflow data with a prescribed shear-stress profile. In: Liu, C., Sakell, L., Beutner, T. (eds.) DNS/LES Progress and Challenges, Proceedings of the Third AFOSR International Conference on DNS/LES, pp. 319–326. Greyden press, Columbus (2001)
32. De Prisco, G., Piomelli, U., Keating, A.: Improved turbulence generation techniques for hybrid RANS/LES calculations. *J. Turbul.* **9**, 1–20 (2008)
33. Laraufe, R., Deck, S., Sagaut, P.: A dynamic forcing method for unsteady turbulent inflow conditions. *J. Comput. Phys.* **230**, 8647–8663 (2011)
34. Roidl, B., Meinke, M., Schröder, W.: Zonal RANS-LES computation of transonic airfoil flow. *AIAA Paper*, AIAA pp 2011–3974 (2011)
35. Roidl, B., Meinke, M., Schröder, W.: A zonal RANS-LES method for compressible flows. *Comput. Fluids* **67**, 1–15 (2012)
36. Bechara, W., Bailly, C., Lafon, P., Candel, S.: Stochastic approach to noise modeling for free turbulent flows. *AIAA J.* **32**, 455–463 (1994)
37. Billson, M., Eriksson, L.-E., Davidson, L.: Jet noise prediction using stochastic turbulence modeling. *AIAA Paper*, AIAA 2003–3282 (2003)
38. Spalart, P.R., Allmaras, S.R.: A one-equation turbulence model for aerodynamic flows. *AIAA Paper*, AIAA 1992–0439 (1992)
39. Menter, F.R.: Zonal two-equation $k-\omega$ turbulence models for aerodynamic flows. *AIAA Paper*, AIAA 1993–2906 (1993)
40. Comte-Bellot, G., Corrsin, S.: Simple Eulerian time correlation of full and narrow-band velocity signals in grid-generated, “isotropic” turbulence. *J. Fluid Mech.* **48**, 273–337 (1971)
41. Batten, P., Goldberg, U., Chakravarthy, S., Batista de Jesus, A.: Large eddy stimulation using simple eddy-viscosity RANS data. In: Eberhardsteiner, J., Böhm, H.J., Rammerstorfer, F.G. (eds.) CD-ROM Proceedings of the 6th European Congress on Computational Methods in Applied Sciences and Engineering (ECCOMAS 2012), September 10–14, 2012, Vienna, Austria (2012)
42. Strelets, M.: Detached eddy simulation of massively separated flows. *AIAA Paper*, AIAA 2001–0879 (2001)
43. Shur, M., Strelets, M., Travin, A.: High-order implicit multi-block Navier-Stokes code: Ten-years experience of application to RANS/DES/LES/DNS of turbulent flows. In: 7th Symposium on Overset Composite Grids & Solution Technology, Huntington Beach, California. http://agarbaruk.professorjournal.ru/c/document_library/get_file?uuid=a8f303a6-ddf5-4f03-9b30-fe11c95b1655&groupId=199655 (2004)
44. Rogers, S.E., Kwak, D.: An Upwind Differencing Scheme for the Time Accurate Incompressible Navier-Stokes Equations. *AIAA Paper*, AIAA 88–2583 (1988)

-
45. Roe, P.L.: Approximate Riemann solvers, parameter vectors and difference schemes. *J. Comput. Phys.* **46**, 357–378 (1981)
 46. Spalart, P.R.: Direct simulation of a turbulent boundary layer upto $Re_\tau = 1440$. *J. Fluid Mech.* **187**, 61–98 (1988)
 47. Schlichting, H.: Boundary Layer Theory. McGraw-Hill Book Co., New York (1960)
 48. Bell, J., Mehta, R.: Development of a two-stream mixing layer from tripped and untripped boundary layers. *AIAA J.* **28**, 2034–2042 (1990)
 49. Greenblatt, D., Paschal, K., Yao, C., Harris, J.: A separation control CFD validation test case. Part 2. Zero efflux oscillatory blowing. *AIAA Paper, AIAA 2005–0485* (2005)
 50. Validation and Improvement of Airframe Noise prediction Tools (VALIANT). <http://www.cimne.com/websasp/valiant/default.asp> Accessed 15 August 2013
 51. Lemoine, B., Roger, M., Legriffon, I.: Aeroacoustics of a model non-lifting wing-flap system in a parallel flow. *AIAA Paper, AIAA 2011–2735* (2011)
 52. Lowson, M.V.: Prediction of Boundary Layer Pressure Fluctuations. Wyle Laboratories Research Staff Report, WR67-15 (1967)
 53. Schewe, G.: On the structure and resolution of wall-pressure fluctuations associated with turbulent boundary-layer flow. *J. Fluid Mech.* **134**, 311–328 (1983)
 54. Bull, M.K.: Wall-pressure fluctuations associated with subsonic turbulent boundary layer flow. *J. Fluid Mech.* **28**, 719–754 (1967)
 55. Goody, M.: Empirical spectral model of surface pressure fluctuations. *AIAA J.* **42**, 1788–1794 (2004)
 56. Shur, M.L., Spalart, P.R., Strelets, M.Kh.: Noise prediction for increasingly complex jets. Part I: Methods and tests. *Int. J. Aeroacoustics* **4**, 213–246 (2005)
 57. Spalart, P.R., Shur, M.L.: Variants of the Ffowcs Williams – Hawkings equation and their coupling with simulations of hot jets. *Int. J. Aeroacoustics* **8**, 477–492 (2009)